HYBRID CONTROLLER FOR VARIABLE SPEED WIND ENERGY CONVERSION SYSTEM WITH SLIP ENERGY RECOVERY USING MATRIX CONVERTER TOPOLOGY

Zakaria KARA , Kamel Barra
Electrical Engineering and Automatic Laboratory
Department of Electrical Engineering ,
Faculty of Sciences and Applied Sciences,
Larbi Ben M'hidi University of Oum Elbouaghi Algeria 04543 ,
CORESSPONDING AUTHOR (Z.Kara: zakkka@yahoo.fr)

Abstract

This paper presents an improved control method of a variable speed Wind Energy Conversion System (WECS). The power conversion chain uses a Doubly Fed Induction Generator (DFIG) supplied via a Matrix Converter (MC) to ensure reliability and good energy conversion management. The proposed hybrid control method combines the merits of Sliding Mode Control (SMC) in term of robustness and high dynamic response in transients to those of Proportional Integral (PI) regulators in term of stability in steady state for constant references. The designed method uses a Fuzzy Logic Supervisor (FLS) that can switches between the two modes according to desired performance. The proposed hybrid controller is applied to track the Maximum Power Point Tracker (MPPT) when wind speed changes abruptly and crucially. The proposed control method provides best efficiency of the conversion chain especially for medium and high power generation systems, also, very attractive results in term of reference tracking and oscillations around Optimal Power Points (OPP) are achieved providing quick and smooth energy conversion. In addition, a unified power factor and low harmonic distortion are also achieved in the grid side.

Keywords (Header1: Abs-Keyw_Ack)

Wind energy conversion system, Doubly fed induction generator, Proportional Integral controller, Matrix Converter, Sliding Mode Control, Fuzzy Logic supervisor, hybrid control.

Symbols

v:	wind speed
J_t:	total inertia coefficient
D:	mechanical dumping factor
G:	gearbox gain
R:	turbine radius
C_p:	aerodynamic efficiency
λ:	Tip Speed Ratio(TSR)
$R_s ; R_r$:	stator and rotor resistances
$L_s ; L_r ; M$	stator; rotor and mutual inductances
$v_i ; v_o$:	input and output voltages of Matrix Converter(MC)
$i_i ; i_o$:	input and output currents of MC
$i_{sa} ; i_{ari} ; i_{ra}$:	stator current, MC input current and MC output current
$i_{sra} ; i'_{sra}$:	current source before and after filtering
P_m, P, Q:	mechanical; active and reactive power
$C1....C8$:	interpolation coefficients for C_p expression
$SAa ; SAb....SCc$:	commutation sequences
$C_f; L_f; R_f$:	filter parameters
$\omega_n; \omega_s ; \xi$:	cutoff and main frequencies, dumping parameter
$\Omega_l; \Omega_h$:	Low Speed Shaft (LSS) and High Speed Shaft (HSS)
T_{em}:	electromagnetic torque

1 Introduction

Nowadays, wind energy conversion has acquired a mature technology and provides a clean and inexhaustible source of energy for maintaining the continuously growing energy needs of humanity.

Wind Energy Conversion System (WECS) can be classified according to speed control and power control ability [1,2]. The speed-control criterion leads to two types of WECS: fixed speed and variable-speed wind turbines. Variable speed wind energy conversion system is the most popular used WECS allowing maximum power extraction over a large range of wind speeds. These WECSs use generally Doubly Fed Induction Generator (DFIG) due to its flexibility, (DFIG can either inject or absorb power from the grid). The stator windings are directly connected to the grid phases providing electric power with constant voltage and frequency, while the rotor windings are connected to back to back voltage source converters (two cascaded converters connected with a direct current DC link). The Rotor Side Converter (RSC) controls the active and reactive power of the generator, while the Grid Side Converter (GSC) controls the DC link voltage and ensures operation of high power factors. As the rotor speed is fluctuating, the electric power of the rotor is reversible depending on whether the machine operates in either subsynchronous mode or supersynchronous mode. Other advantages of DFIG machines can be cited, such as the adaptability of the power factor, better efficiency, ability to control the reactive power without capacitive support, significant reduction of the power converters size and cost since the size of the converter is related to the speed variation range, typically around +/- 30% of the synchronous speed. Note that the main advantage of the WECS based DFIG machine is the perfect decoupling between active and reactive power control by controlling rotor currents [1,3,4].

During the two last decades, several control strategies for WECSs based DFIG have been reported in specialist literature starting from the basic idea that control does significantly improve all aspects of WECSs. The most widely used technique is Field Oriented Control (FOC) [4,5,6] where rotor currents are decomposed into direct component that controls the torque (the stator active power) and a quadrature component that commands the rotor flux (stator reactive power) and they are regulated separately with linear PI regulators. The block diagram of the power control of the DFIG incorporates, generally, a cascaded structure with four PIs regulators, two PIs in the outer loops for stator active and reactive powers, and two PIs in the inner rotor currents loops. An additional MPPT controller for speed tracking is added. Simplified structures have been then proposed by eliminating sometimes inner currents loops and sometimes the outer power loops but at least the control block contains three PIs controllers [4,5,6].

The maximum energy capture available in the wind generator can be achieved if the turbine rotor operates on the Optimal Regime Characteristic (ORC). This regime can be obtained by tracking some target variables: the optimal rotational speed, depending proportionally on the wind speed, and the optimal rotor power [1].

In this way, the standard PI control is widely used in WECS, owing its popularity to some key features such as its simple design procedure, easy to implement, it requires little feedback information, and especially for its best tracking performance in steady state [1,5,6,7].

As it is well known that wind speed in WECS is very fluctuating and changes abruptly due to external atmospheric conditions, the external wind speed loop needs to be controlled with robust and fast controllers such as sliding mode controller (SMC).

In this paper, we investigate by numerical simulation the role played by the maximum power point tracking (MPPT) controller in a variable speed WECS to control the power conversion. To reduce the cost of the conversion chain, the standard converter topology that uses two back to back converters is replaced by a matrix converter (MC) topology ensuring operation at large power factor. Therefore, the MC is connected to the grid phases throw an input filter (Lf , Rf , Cf) to avoid overvoltages generation and to eliminate high-frequency harmonics in grid currents.

The global control scheme of the studied system is given in figure 1. The MPPT controller is used to track closely the maximum power point tracker of the wind turbine (turbine rotor works closely on the optimal regime characteristic ORC), then two PIs controllers are used to control separately the active and reactive power of the DFIG. The MC modulation technique is space vector

modulation (SVM) well adequate for such application due to its low harmonic distortion and its constancy switching frequency. Note that one of the benefits of the present work is that both stator and MC converter are connected to the grid via a filter designed to avoid overvoltages and current harmonics.

The performance of the maximum power point tracking stage are simulated and given for three kinds of controllers, standard PI controller, sliding mode controller (SMC) and hybrid PI-SMC based fuzzy supervisor controller. The hybrid PI-SMC based fuzzy supervisor is synthesized in order to keep the SMC robustness, the high dynamic response in transients and to eliminating the torque ripples (mechanical stress) due to chattering phenomenon in steady state.

2 Modelling of the studied system

2.1 Wind speed model

Wind dynamics result from combining meteorological conditions with particular features of a given site. Wind speed is modelled in the literature as a non-stationary random process, yielded by superposing two components [1]:

$$v(t) = v_s(t) + v_t(t) \qquad (1)$$

$v_s(t)$ is the low-frequency component (describing long term, low-frequency variations) and $v_t(t)$ is the turbulence component (corresponding to fast, high frequency variations)

The profile of wind speed is depicted in figure 2 for duration of 5 s, only the non-stationary component wind speed is used.
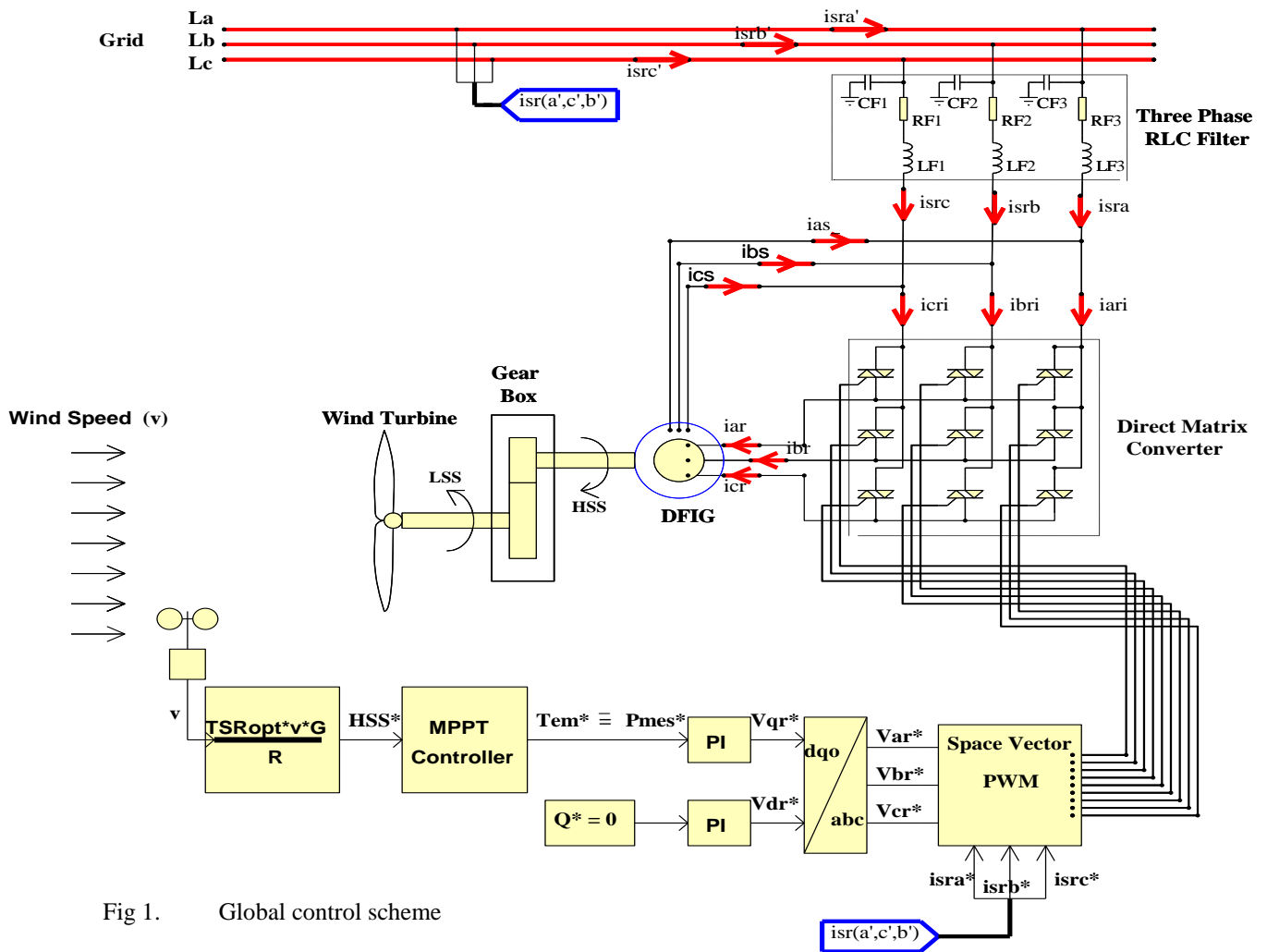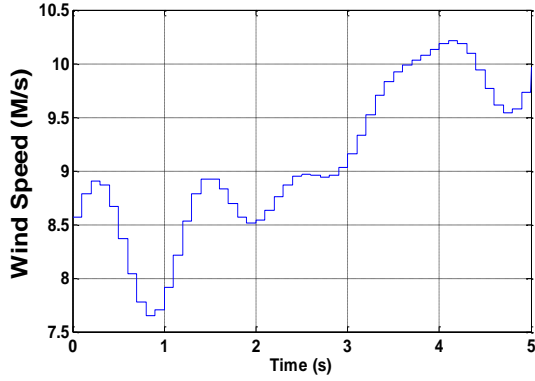

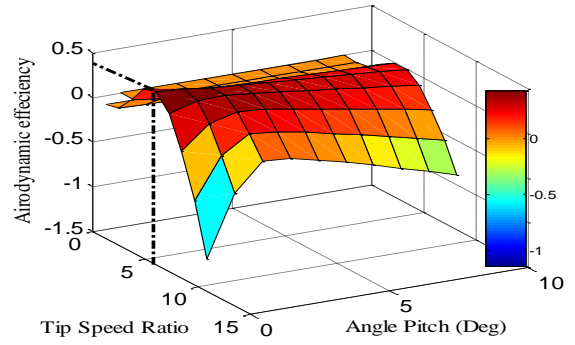Fig 1. Global control scheme

Fig 2. Profile of the wind speed v(t)

Fig 3. Aerodynamic efficiency versus tip speed ratio and pitch angle

2.2 Wind turbine characteristics

The configuration studied in the present paper is a fixed pitch horizontal axis wind turbines (HAWT) having an aerodynamic efficiency Cp depending on the tip speed ratio (TSR) (i.e., the ratio between the blades' peripheral speed and the wind speed: $\lambda=\Omega.R/ v$) and having a maximum for λopt for a well-determined value. The power characteristics of the wind turbine have a maximum for each wind speed. All these maxima form the so-called optimal regimes characteristics (ORC). The available power on the turbine shaft is [1,5]:

$$P_m = \frac{1}{2}C_p(\lambda) \cdot \rho \cdot \pi R^2 \cdot v^3 \qquad (2)$$

The power coefficient Cp is then given by [5]:

$$C_p(\lambda,\beta) = C_1(\frac{C_2}{\lambda_i} - C_3\beta - C_4\beta^{C_5} - C_6) \cdot exp(\frac{-C_7}{\lambda_i}) \qquad (3)$$

$$\begin{cases} \frac{1}{\lambda_i} = \frac{1}{\lambda + C_8\beta} - \frac{C_9}{\beta^3 + 1} \\ \lambda = \frac{R\Omega}{v} \end{cases} \qquad (4)$$
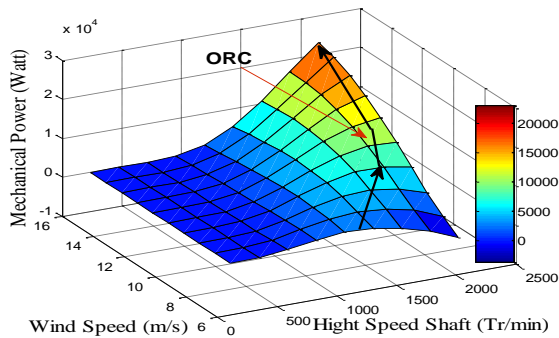

Fig 1. Captured power versus wind speed and high speed shaft.

Figure 3 gives a 3D plot of the mechanical power captured by the wind turbine versus wind speed and high speed shaft whereas figure 4 depicts a 3D plot of aerodynamic efficiency *Cp* versus tip speed ratio λ for different values of the pitch angle β.

2.3 DFIG Model

The equations that describe a doubly fed induction generator (DFIG) in a d-q reference frame, where different parameters of the machine appears in a continue form, are identical to those of a squirrel cage induction generator; the only exception is that the rotor winding is not short-circuited. Here, we assume balanced voltages and non-ground connection points. The stator and rotor voltages are given by the following equations [4,6]:

$$\begin{cases} V_{ds} = R_s i_{ds} + \frac{d\psi_{ds}}{dt} - \omega_s\psi_{qs} \\ V_{qs} = R_s i_{qs} + \frac{d\psi_{qs}}{dt} + \omega_s\psi_{ds} \\ V_{dr} = R_r i_{dr} + \frac{d\psi_{dr}}{dt} - \omega_{sl}\psi_{qr} \\ V_{qr} = R_r i_{qr} + \frac{d\psi_{qr}}{dt} + \omega_{sl}\psi_{dr} \end{cases} \qquad (5)$$

The electromagnetic torque is expressed as:

$$T_{em} = p(\psi_{ds}i_{qs} - \psi_{qs}i_{ds}) \qquad (6)$$

where V_{ds}, V_{qs}, i_{ds}, i_{qs}, ψ_{ds}, ψ_{qs}, V_{dr}, V_{qr}, i_{dr}, i_{qr}, ψ_{dr}, ψ_{qr} are voltage components, current components and flux components of stator and rotor, respectively. The flux components are given by:

$$\begin{cases} \psi_{ds} = L_s i_{ds} + M i_{dr} \\ \psi_{qs} = L_s i_{qs} + M i_{qr} \end{cases}$$

$$\begin{cases} \psi_{dr} = L_r i_{dr} + M i_{ds} \\ \psi_{qr} = L_r i_{qr} + M i_{qs} \end{cases} \tag{7}$$

In order to obtain a decoupled control of stator active-reactive powers, the DFIG model requires all quantities to be expressed under stator flux orientation concept, and assuming that the stator resistance is small when compared to the stator reactance for medium and high power size machine, the stator flux can be computed as [1,4,6]:

$$\begin{cases} \psi_{ds} \approx \psi_s \approx \dfrac{V_s}{\omega_s} \\ \psi_{qs} = 0 \end{cases} \tag{8}$$

After some manipulations, we can get from (5),(7) and (8) the stator current expressions by:

$$\begin{cases} i_{ds} = \dfrac{\psi_s}{L_s} - \dfrac{M}{L_s} i_{dr} \\ i_{qs} = -\dfrac{M}{L_s} i_{qr} \end{cases} \tag{9}$$

The stator active-reactive powers expressions are given then by:

$$\begin{cases} P_s = V_{ds} i_{ds} + V_{qs} i_{qs} = -V_s \dfrac{M}{L_s} i_{qr} \\ Q_s = V_{qs} i_{ds} - V_{ds} i_{qs} = \dfrac{V_s^2}{\omega_s L_s} - \dfrac{V_s M}{L_s} i_{dr} \end{cases} \tag{10}$$

Relations (10) mean that the resulting system binds proportionally the stator active power to rotor q-axis current component and the stator reactive power to the rotor d-axis current component.

The expression for the electromagnetic torque becomes:

$$T_{em} = -p \frac{M}{L_s} i_{qr} \psi_{ds} = \frac{p}{\omega_s}\left(-V_s \frac{M}{L_s} i_{qr}\right) = \frac{p}{\omega_s} P \tag{11}$$

The rotor voltage expressions are then simplified as:

$$\begin{cases} V_{dr} = R_r\, i_{dr} + \sigma L_r \dfrac{di_{dr}}{dt} - g\,\omega_s \sigma L_r i_{qr} \\ V_{qr} = R_r\, i_{qr} + \sigma L_r \dfrac{di_{qr}}{dt} + g\,\omega_s \sigma L_r i_{dr} + g\,\dfrac{MV_s}{L_s} \end{cases} \tag{12}$$

2.4 Matrix Converter Model

Matrix Converter is a direct AC–AC converter that uses an array of (m x n) controlled bi-directional switches to directly connect m-phase inputs to n-phase outputs. Matrix Converters (MC) have received a considerable attention these last years because of their numerous merits on the traditional AC-DC-AC converters such as no DC-link capacitor, the bi-directional power flow control (the capability of regeneration), the sinusoidal input-output waveforms and adjustable input power factor, but the biggest drawback of this technology is the high control complexity [7,8,9,10].
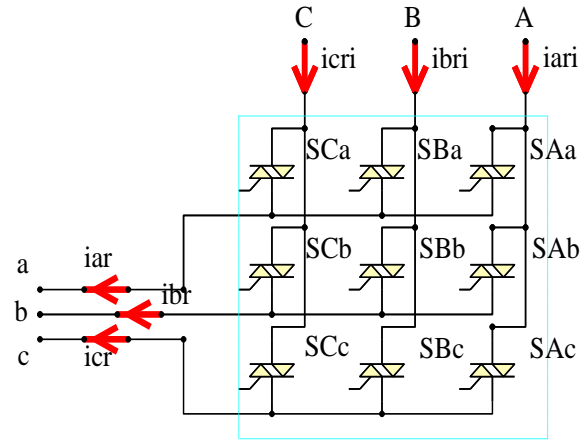

Fig 4.   Topology of matrix converter

The load current must not be interrupted abruptly, because of the inductive nature of the load that can generate an important overvoltage destroying the components. In addition, operation of the switches cannot short-circuit two input lines, because this switching state will originate short circuit currents. These two restrictions can be expressed in mathematical form by the following equation:

$$S_{Ay} + S_{By} + S_{Cy} = 1 \quad \forall \quad y \in \{a,b,c\} \tag{13}$$

Referenced to the neutral point N, the relation between the load and input voltages of the MC is expressed as:

$$\begin{bmatrix} v_{ao}(t) \\ v_{bo}(t) \\ v_{co}(t) \end{bmatrix} = \underbrace{\begin{bmatrix} S_{Aa} & S_{Ba} & S_{Ca} \\ S_{Ab} & S_{Ba} & S_{Ca} \\ S_{Ac} & S_{Ba} & S_{Ca} \end{bmatrix}}_{T} \times \begin{bmatrix} v_{ai}(t) \\ v_{bi}(t) \\ v_{ci}(t) \end{bmatrix} \tag{14}$$

where T is the instantaneous transfer matrix. The input and load voltages can be expressed as vectors as follows:

$$v_o = \begin{bmatrix} v_{ao}(t) \\ v_{bo}(t) \\ v_{co}(t) \end{bmatrix} \quad v_i = \begin{bmatrix} v_{ai}(t) \\ v_{bi}(t) \\ v_{ci}(t) \end{bmatrix} \tag{15}$$

the relation of the voltages is given by

$$v_o = T \times v_i \tag{16}$$

Then, the following equation can be obtained for rotor quantities:

$$\begin{bmatrix} i_{ari}(t) \\ i_{bri}(t) \\ i_{cri}(t) \end{bmatrix} = \underbrace{\begin{bmatrix} S_{Aa} & S_{Ab} & S_{Ac} \\ S_{Ba} & S_{Ba} & S_{Ba} \\ S_{Ca} & S_{Ca} & S_{Ca} \end{bmatrix}}_{T^T} \times \begin{bmatrix} i_{ar}(t) \\ i_{br}(t) \\ i_{cr}(t) \end{bmatrix} \tag{17}$$

Considering the current vectors

$$i_o = \begin{bmatrix} i_{ar}(t) \\ i_{br}(t) \\ i_{cr}(t) \end{bmatrix} \quad\quad i_i = \begin{bmatrix} i_{ari}(t) \\ i_{bri}(t) \\ i_{cri}(t) \end{bmatrix} \tag{18}$$

The equation for the current is

$$i_i = T^T \times i_o \tag{19}$$

where T^T is the transposed of matrix T.

2.5 The Indirect Space Vector Modulation

The SVM strategy, based on space vector representation becomes very popular due to its simplicity, low harmonic distortion and constancy of switching frequency. In contrast to sinusoidal PWM, SVM treats the three phase quantities as a single equation known as reference space vector given by [7,9,11]:

$$v^* = \tfrac{2}{3}\left(v_{ao}^*(t) + v_{bo}^*(t) \cdot e^{j2\pi/3} + v_{co}^*(t) \cdot e^{-j2\pi/3} \right) \tag{20}$$

The main idea of the indirect modulation technique is to consider the matrix converter as a two-stage transformation converter: a rectification stage to provide a constant virtual dc-link voltage Upn during the switching period by mixing the line-to-line voltages in order to produce sinusoidal distribution of the input currents, and an inverter stage to produce the three output voltages. Figure 6 shows the converter topology when the indirect modulation technique is used.
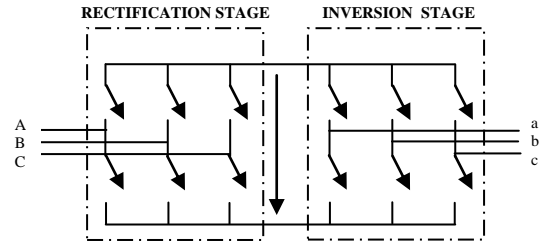

Fig 5. The matrix converter model when an indirect modulation technique is used [7] .
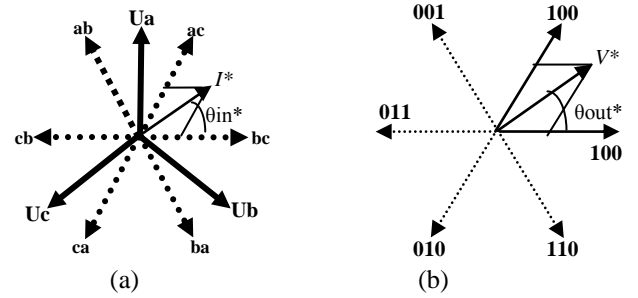

(a)   (b)

Fig 6. Generation of the reference vectors using SVM: (a) rectification stage; (b) inversion stage [7]

By multiplying the rectification stage matrix R by the inversion stage matrix I, the converter transfer matrix T is obtained:

$$T = R \cdot I$$

$$\underbrace{\begin{bmatrix} S_{Aa} & S_{Ba} & S_{Ca} \\ S_{Ab} & S_{Ba} & S_{Ca} \\ S_{Ac} & S_{Ba} & S_{Ca} \end{bmatrix}}_{T} = \begin{bmatrix} S_A \\ S_B \\ S_C \end{bmatrix} \cdot \begin{bmatrix} S_a & S_b & S_c \end{bmatrix} \tag{21}$$

This technique uses a combination of the two adjacent vectors and a zero vector to produce the reference vector. The proportion between the two adjacent vectors gives the direction and the zero-vector duty cycle determines the magnitude of the reference vector. The input current vector that corresponds to the rectification stage of figure 7.a and the output voltage vector that corresponds to the inversion stage of figure 7.b are the reference vectors.

In order to implement the SVM, it is necessary to determine the position of the two reference vectors. The input reference current vector I_i^* is given by the input voltage vector if an instantaneous unitary power factor is

desired, or it is given by a custom strategy to compensate for unbalanced and distorted input voltage system. The output reference voltage vector V_o* may be produced by the active and reactive powers control scheme.

When the absolute positions of the two reference vectors yin and yout are known, the relative positions inside the corresponding sector $\theta_{in}*$ in and $\theta_{ou}*$ out, as well as the sectors of the reference vectors, are determined [7]:

$$in_{sec} = trunc\left(\frac{\theta_{in}}{\pi/3}\right)$$
$$out_{sec} = trunc\left(\frac{\theta_{out}}{\pi/3}\right) \tag{22}$$

$$\theta^*_{in} = \theta_{in} - \pi/3 \cdot in_{sec}$$
$$\theta^*_{out} = \theta_{out} - \pi/3 \cdot out_{sec} \tag{23}$$

The duty cycles of the active switching vectors are calculated for the rectification stage by using the following relations:

$$d_\gamma = m_i \cdot sin\left(\pi/3 - \theta^*_{in}\right)$$
$$d_\delta = m_i \cdot sin\left(\theta^*_{in}\right) \tag{24}$$

and for the inversion stage by:

$$d_\alpha = m_v \cdot sin\left(\pi/3 - \theta^*_{out}\right)$$
$$d_\beta = m_v \cdot sin\left(\theta^*_{out}\right) \tag{25}$$

where mi and mv are the rectification and inversion stage modulation indexes, and $\theta_{in}*$ and $\theta_{out}*$ are the angles within their respective switching hexagon of the input current and output voltage reference vectors. Usually,

$$m_i = 1 , m_v = \frac{\sqrt{3} \cdot v_o}{V_{mn}} \tag{26}$$

where v_o is the magnitude of the output reference voltage vector and U_{pn} is the virtual dc-link voltage. In the ideal sinusoidal and balanced input voltages, the virtual dc-link voltage remains constant:

$$V_{mn} = d_\gamma \cdot v_{line-\gamma} + d_\delta \cdot v_{line-\delta} = 0.86 \cdot \sqrt{2} \cdot v_{line} \tag{27}$$

where $v_{line-\gamma}$ and $v_{line-\delta}$ are the instantaneous values of the two line-to-line voltages to be combined in the switching period to produce the virtual dc-link and v_{line} is

the magnitude of the line-to-line voltage system. Then, to obtain a correct balance of the input currents and the output voltages, the modulation pattern should be a combination of all the rectification and inversion duty-cycles ($\alpha\gamma$ – $\alpha\delta$ - $\beta\delta$ – $\beta\gamma$ - 0). The duty cycle of each sequence is determined as a product of the corresponding duty cycles:

$$d_{\alpha\gamma} = d_\gamma \cdot d_\alpha ; \ d_{\beta\delta} = d_\beta \cdot d_\delta$$
$$d_{\alpha\delta} = d_\alpha \cdot d_\delta ; \ d_{\beta\gamma} = d_\beta \cdot d_\gamma \tag{28}$$

The duration of the zero vectors is calculated by

$$d_0 = 1 - \left(d_{\alpha\gamma} + d_{\alpha\delta} + d_{\beta\delta} + d_{\beta\gamma}\right). \tag{29}$$

The duration of each sequence is calculated by multiplying the corresponding duty cycle by the switching period.

2.6 Input Filter Model

The input filter is very important to reduce current ripples and overvoltages with minimum installed energy on the reactive elements [7,9].

The input filter model, based on the circuit shown in Figure 8, can be described by the following continuous-time equations [9,10,11]:
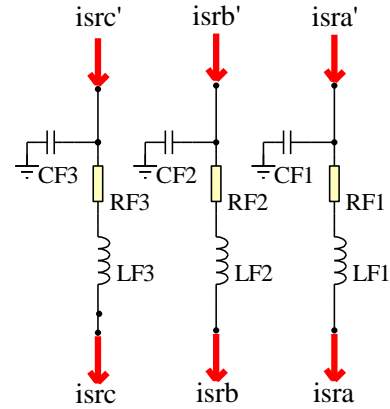

Fig 7.   Single Stage input filter

$$v_s(t) = R_f i_s(t) + L_f \frac{i_s(t)}{t} + v_i(t) \tag{30}$$

$$i_s(t) = i_i(t) + C_f \frac{v_i(t)}{t} \tag{31}$$

where Lf , Rf , Cf are the inductance, resistance and capacitance of the filter. The design of the input filter has

to accomplish the following [7,9]:

-Produce an input filter with a cutoff frequency lower than the switching frequency, and higher than the fundamental frequency of the input AC source

$$\omega_n = \frac{1}{\sqrt{C_f L_f}} \qquad (32)$$

$\omega_0 = 2\pi f_0$ is the resonance pulsation of the input filter.

-The input power factor should be kept maximum for a given minimum output power:

$$\frac{C_f}{P_{MCn}} = k_{min} \cdot tan(\varphi_{min}) \frac{1}{3 \cdot \omega_s \cdot V_n} \qquad (33)$$

where $P_{MCn} = 3. Vn. In$ is the rated input active power (considering a close to unity power factor at full load). Vn; In are the rated input phase voltage and current of the converter; $P_{MC-min} = k_{min} . P_{MCn}$ is the minimum power level where the displacement angle φ_{min} reaches its limit and $\omega_s = \omega_n = 2\pi f_n$ is the pulsation of the grid.

-Minimize the input filter volume or weight for a given reactive power, by taking into account the energy densities which are different for film capacitors than for iron chokes:

$$\frac{S_{Lf}}{S_{Cf}} = \frac{1}{[3 \cdot \omega_n \cdot Vn]} \left(\frac{P}{C_f} \right)^2 \qquad (34)$$

Where S_{Lf} (choke) , S_{Cf} (capacitor) are the installed VA in reactive components.

-The voltage drop in the inductor should be minimum to provide the highest voltage transfer ratio::

$$\frac{\Delta V}{V_n} = 1 - \sqrt{1 - (\omega_s \cdot L_f)^2 \cdot \left(\frac{I_n}{V_n} \right)^2} \qquad (35)$$

The Bode diagram of the designed filter is plotted in figure 9, where the main frequency (60 Hz) is dashed in blue and the dominant frequency which is switching frequency (1.1 kHz) is in red, however cutoff frequency of the filter (1kHz) is in green color having a dumping factor of ξ=0.5.
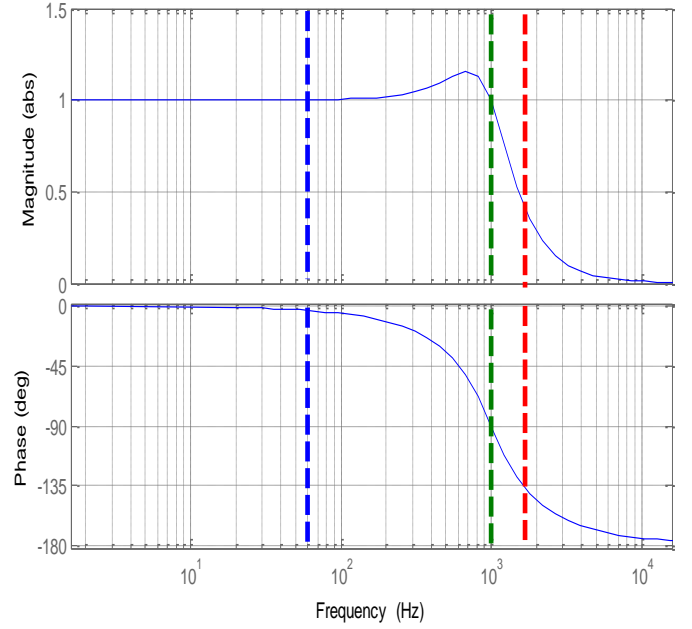
Fig 8.　　Main characteristics of the designed filter

3 Control strategy

Control of variable-speed fixed-pitch WECS in the partial load regime generally aims at regulating the power harvested from wind by modifying the electrical generator speed. For each wind speed, there is a certain rotational speed at which the power curve of a given wind turbine has a maximum (Cp reaches its maximum value).

All these maxima compose what is known in the literature as the Optimal Regimes Characteristic, ORC[1]

To ensure an optimal regime it must manipulate the aerodynamic efficiency coefficient by regulating the speed generator in order to keep Cp(t,λ)= Cpmax=Cp(λopt) this is effectuated by injecting a speed set point derived from the relation (37) then a torque set point is generated. From the relationship between the torque and active power (11), a set point for the generated power is derived.

3.1 MPPT and regulator synthesis

The DFIG torque is controlled to maintain the tip speed ratio in its optimal value. The speed set point is derived from the optimal tip speed ratio as:

$$\begin{cases} \Omega = \Omega_h^* = \Omega_l^* \, G \\ \Omega_l^* = \dfrac{\lambda_{opt} \, v(t)}{R} \end{cases} \tag{37}$$

So the MPPT regulator is implement to control the turbine mechanical speed. For this purpose, two regulation modes are developed and are compared, then we have proposed a combination mode which allow us to keep advantages and to eliminate disadvantages of each one between the previous modes.

a) PI control

From system parameters (D,Jt)are positives values one can deduce the stability of our system. The aim of the
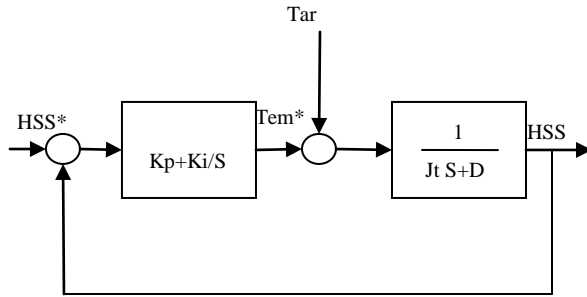
Fig 9.   PI Control scheme

Proportional Integral regulator here is to ameliorate the system time response. The figure (10) illustrates the control diagram using the PI regulator

The closed loop transfer function is :

$$H(S) = \frac{K_p \cdot s + K_i}{J_t \cdot s^2 + (D + K_p) \cdot s + K_i} \tag{38}$$

In order to obtain a desired first order system behaviour :

$$H(S) = \frac{1}{\tau s + 1} \tag{39}$$

the controller parameters' are expressed as :

$$K_p = \frac{J_t}{\tau}, \; K_i = \frac{D}{\tau}$$

b) The sliding mode controller

Computation of the sliding surface and of the sliding-mode control law starts from the state equations in the form[2]

$$\dot{x} = f(x,t) + b(x,t) \cdot u$$

$$x = \begin{bmatrix} \Omega_h \; T_{em} \end{bmatrix}$$

$$f(x) = \begin{bmatrix} T_{ar}(\Omega_h, v) / J_t - T_{em} / J_t & -T_{em} / \tau_{ems} \end{bmatrix}^T$$

$$b(x,t) = \begin{bmatrix} 0 \; 1 / \tau_{ems} \end{bmatrix}$$

$$u = T_{em}^*.$$

The sliding mode dynamics may be imposed as equivalent to some linear ones[2].

$$\dot{\Omega} = \frac{T_{ar}(\Omega_h, v) - T_{em}}{J_t} \equiv \begin{bmatrix} c_1 \; c_2 \end{bmatrix} \begin{bmatrix} \Omega \; T_{em} \end{bmatrix}^T \tag{40}$$

* **Sliding Surface**

Let s(x,u,t) denote the sliding surface. The condition:

$$\frac{\partial s}{\partial x} \cdot b(x,t) = 0$$

existence of the equivalent control input –, require that:

$$\frac{\partial s}{\partial T_{em}} = c \neq 0$$

a first form of the switching surface may be written:

$$s(\Omega_h, T_{em}) = s(\Omega_h) + c \cdot T_{em} \tag{41}$$

And when the sliding surface is reached

$$s(\Omega_h, T_{em}) = s(\Omega_h) + c \cdot T_{em} = 0$$

So:

$$s(\Omega_h) = -c \cdot T_{em} \tag{42}$$

Then from equation 26

$$T_{em} = \frac{1}{1 + c_2 \cdot J_t} \left(T_{ar}(\Omega_h, v) - c_1 \cdot J_t \cdot \Omega_h \right) \tag{43}$$

Here one can deduce that

$$c = 1 + c_2 \cdot J_t$$

Equations 43 and 42, combined with Equation 26, gives the expression of the sliding surface [2]:

$$s(\Omega_h, T_{em}) = c_1 \cdot J_t \cdot \Omega_h + (1 + c_2 \cdot J_t) T_{em} - T_{ar}(\Omega_h, v)$$
$$= c_1 \cdot J_t \cdot \Omega_h + (c_2 \cdot J_t) T_{em} + T_{em} - T_{ar}(\Omega_h, v)$$

$$T_{em} - T_{ar}(\Omega_h, v) = J_t \cdot \dot{\Omega}_h$$

$$s(\Omega_h, T_{em}) = c_1 \cdot J_t \cdot \Omega_h + (c_2 \cdot J_t) T_{em} + J_t \cdot \dot{\Omega}_h \tag{44}$$

* **Sliding-mode Control Law**

Now the two components of the sliding mode control law are computed : the equivalent control input, u_{eq} , and the on-off component, U_N.

To compute the equivalent control input the following relation is used:

$$u_{eq} = -\left[\frac{\partial s}{\partial x} b\right]^{-1} \cdot \left[\frac{\partial s}{\partial t} + \frac{\partial s}{\partial x} \cdot f(x,t)\right] \qquad (45)$$

We compute part by part :

$$\left[\frac{\partial s}{\partial x} b\right]^{-1} = \left[\left[\frac{\partial s}{\partial \Omega_h} \quad \frac{\partial s}{\partial T_{em}}\right] \cdot \left[\begin{matrix} 0 \\ 1/\tau_{ems} \end{matrix}\right]\right]^{-1}$$

$$= \left[\frac{1}{\tau_{ems}} \frac{\partial s}{\partial T_{em}}\right]^{-1} = \left[\frac{1 + c_2 \cdot J_t}{\tau_{ems}}\right]^{-1}$$

$$= \frac{\tau_{ems}}{1 + c_2 \cdot J_t} \qquad (46)$$

$$\frac{\partial s}{\partial t} = 0 \qquad (47)$$

$$\frac{\partial s}{\partial \Omega_h} = c_1 \cdot J_t - \frac{1}{\tau_{ems}} \cdot \frac{\partial T_{ar}}{\partial \Omega_h}$$

$$\frac{\partial T_{ar}}{\partial \Omega_h} = 0.5\pi\rho R^3 v^2 \frac{\partial(C_P(\lambda)/\lambda)}{\partial \Omega_h}$$

$$= Qv^2 \frac{\partial(C_P(\lambda)/\lambda)}{\partial \lambda} \frac{\partial \lambda}{\partial \Omega_h} \qquad (48)$$

where $Q = 0.5\pi\rho R^3$

$$\frac{\partial(C_P(\lambda)/\lambda)}{\partial \lambda} = \frac{\lambda \cdot C_P^{\cdot}(\lambda) - C_P(\lambda)}{\lambda^2}$$

$$\frac{\partial \lambda}{\partial \Omega_h} = \frac{R}{G \cdot v} \quad / \quad \partial \Omega_h = G \cdot \partial \Omega_L$$

$$\frac{\partial s}{\partial \Omega_h} = c_1 \cdot J_t - \frac{Q \cdot R \cdot v}{\tau_{ems} \cdot G}\left(\frac{\lambda \cdot C_P^{\cdot}(\lambda) - C_P(\lambda)}{\lambda^2}\right) \qquad (49)$$

$$\frac{\partial s}{\partial T_{em}} = 1 + c_2 \cdot J_t \qquad (50)$$

By replacing each one of equations 46, 48, 49 and 50 in the equation 45 of the equivalent control input, one obtains after some algebra:

$$u_{eq} = T_{em} - \frac{\tau_{ems}}{1 + c_2 \cdot J_t} \cdot$$

$$\left[\left(c_1 \cdot J_t - \frac{QRv}{G}\frac{\lambda \cdot C_P^{\cdot}(\lambda) - C_P(\lambda)}{\lambda^2}\right)(c_1\Omega + c_2 T_{em})\right] \qquad (51)$$

Parameter c_1 is chosen to impose the convergence speed to the sliding mode regime: $c_1 = -1/\tau_{sd}$ where the time constant $\tau_{sd} > 0$. The value of c2 results from imposing the "target" steady state as being the Optimal operating point (OOP), corresponding to λopt :

$$\dot{\Omega} = c_1\Omega_{opt} + c_2 T_{opt} = 0$$

$$c_2 = -c_1 \frac{\Omega_{opt}}{T_{opt}} \qquad (52)$$

c_1 is the negative inverse of the time constant and c_2 is the (static) gain. One may attempt to dynamically modify c_2, using the following expression[2] :

$$c_2 = -c_1 \frac{\Omega_{opt}}{T_{opt}\left(1 + K\frac{(\Omega - \Omega_{opt})}{\Omega_{opt}}\right)} \qquad (53)$$

Where K > 0 as a tradeoff parameter

The nonlinear control component U_N (on-off) is chosen as:

$$U_N = -A \cdot sign_\Delta(s)$$

$$A > 0 \qquad (54)$$

Δ : the hysteresis band

figures (11) to (12) illustrate a comparative show for the High Speed Shaft (Ω) tracking and Electromagnetic Torque (Tem) Tracking for each control mode (PI & SMC).
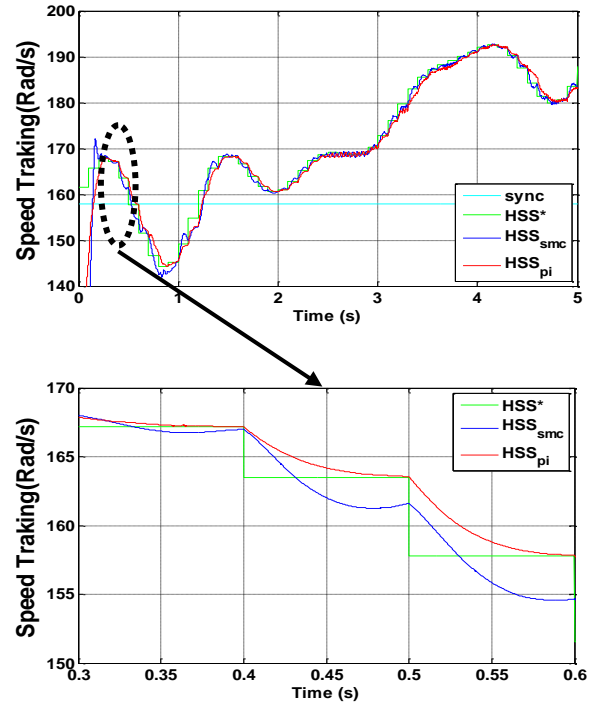

Fig 10.   High Speed Shaft (HSS) tracking for both PI and SMC controllers.
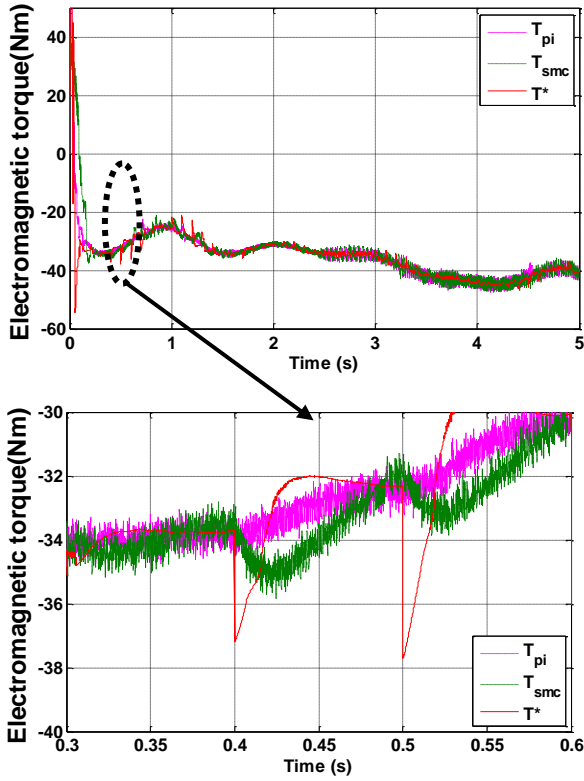
Fig 11.   Torque Tracking performance for both PI and SMC controllers

The performance of the MPPT tracking control is tested for both PI and SMC controllers for the wind speed profile of figure 2. One can see easily that the SMC provide high dynamic performance in transients than PI but it oscillates in steady state around its reference due to chattering phenomenon causing mechanical stress, losses in the power conversion chain, and undesirable ripples on electromagnetic torque, whereas, the PI controller gives best performance in steady state with stable profile.

c)   Hybrid control

The main contribution of our work is to design a new hybrid control that combines the merits of the two precedent controllers. The hybrid control uses a fuzzy logic supervisor that switches between the two modes according to desirable performance.

The inputs of the proposed supervisor are basically the speed tracking error (e) and its variation (de). The law combining between the PI and SMC commands uses the following expression:

$$U = \delta \times U_{PI} + (1 - \delta) \times U_{SMC} \qquad (55)$$
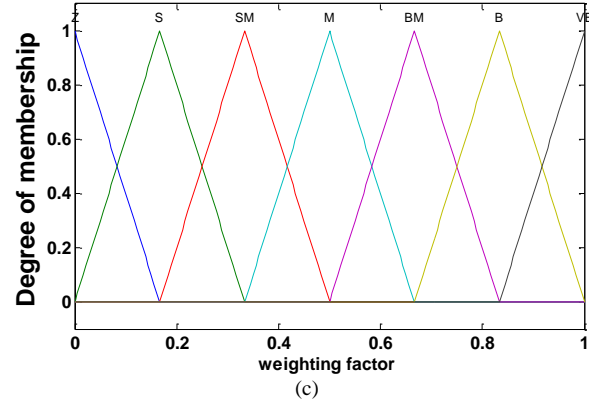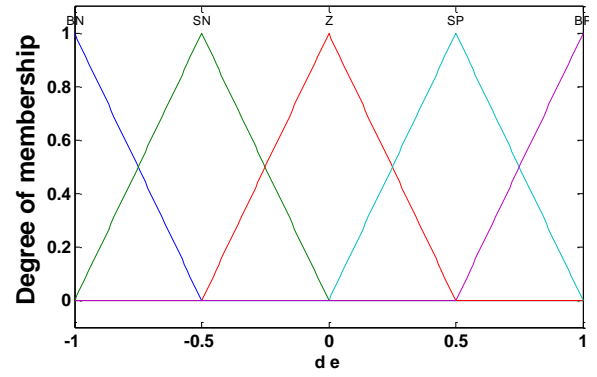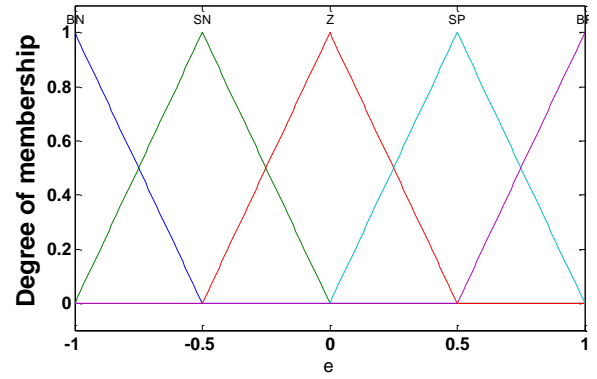
Fig 12.   (a), (b) Error fuzzification and its variation, (c) Output defuzzification.
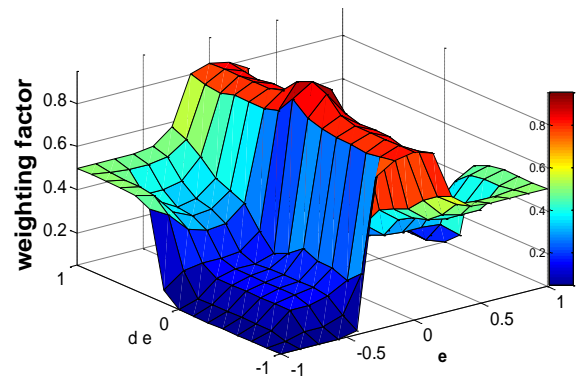
Fig 1.   The Surface evoked by the supervisor.

Where δ is a weighting factor generated by the fuzzy supervisor. The base rules are chosen in order to get $\delta = 0$ when the system is far from the OPP; and $\delta = 1$ when the system reaches the new OPP.

Figure (13) depict (a) the speed error, (b) the error variation and (c) the weighting factor, whereas figure (14) illustrates the surface generated by the supervisor

3.2 Power control

The schematic control of the studied power system is illustrated by figure (1); where the active power set point is derived from torque reference signal witch results from the speed tracking loop however the reactive power is settled to 0 in order to keep a unity power factor in the generated power:

$$\begin{cases} P^* = \dfrac{\omega_s}{p} T_g^* \\ Q^* = 0 \end{cases} \qquad (56)$$

The both active-reactive power PI regulators are synthesized by the same manner of speed PI regulator, and the system regulated is the described one in the 12 equations set

4 Simulation results

The numerical simulations of the proposed hybrid controller are evaluated on Matlab-Simulink hardware for the wind speed profile depicted in figure 2 for both sub-synchronous mode and super-synchronous mode.

Figures from 15 to 18 illustrate the high speed shaft (HSS) tracking if the DFIG, the electromagnetic torque, the tip speed ratio λ and the aerodynamic efficiency Cp for both controllers: Hybrid, SMC and PI. It can be seen that the performance of the proposed hybrid controller are relevant compared to those of SMC and PI controllers, especially in term of fast transient duration, good robustness, stability in steady state and low torque ripples.

The two most energy conversion quality indicating parameters (Cp,λ) are also depicted and they show clearly the high performance of the proposed controller since they oscillate closely around their optimal values providing high efficiency of the conversion chain.

Figure 20 illustrates the stator active and reactive powers injected in the grid, where the reference reactive power is settled to 0 in order to get a unity power factor, however, figure 19 shows the fluctuation of the fuzzy supervisor decision (δ) that switches between the two modes.

Figures from 21 to 23 illustrate the rotor line to line voltage (vabr), the stator current (ias), the MC input current (i_{ari}) and the rotor current (i_{ar}) . On these figures one can see that all these quantities follow the variations of the wind speed profile and the WECS works at unity power factor since the stator reactive power is fluctuating around 0 as can be seen in figure 18.

Figure 24 depicts the MC input voltage (v_{ari}) versus current (i_{ari}) for both sub-synchronous regime (case a) and hyper-synchronous regime (case b), where we can see for the sub-synchronous mode that the current is in phase with the voltage meaning that the slip power flows from the grid to the DFIG via matrix converter, and when the machine operates in the super-synchronous mode, the current turns in opposite phase with the voltage meaning that the slip power flows from the DFIG rotor to the grid via the matrix converter.

To see the role played by the designed filter, we have compared the profile of the unfiltered current (i_{sra}) and voltage (v_{sra}) before connecting with the grid (see figure25) to filtered ones (isra'), (vsra') after connecting with the grid (figure 28). One can see that a significant power quality enhancement is achieved by the RLC filter proofed by the THD, where it is observed in figure 29 and in figure 30 that the THD is reduced from THD$isra$=0.4808 (48%) for the unfiltered current to THD$isra'$=0.0482 (4.82%) for the filtered current by eliminating all harmonics that appear in the grid current specter.
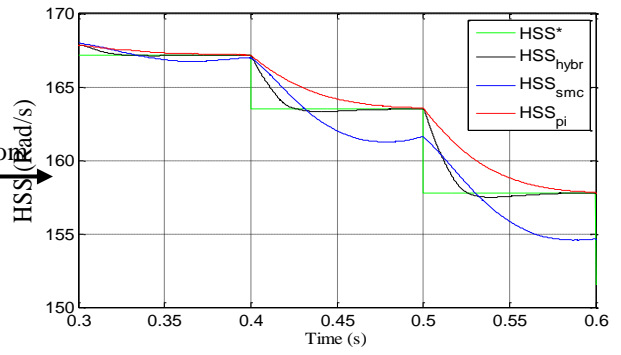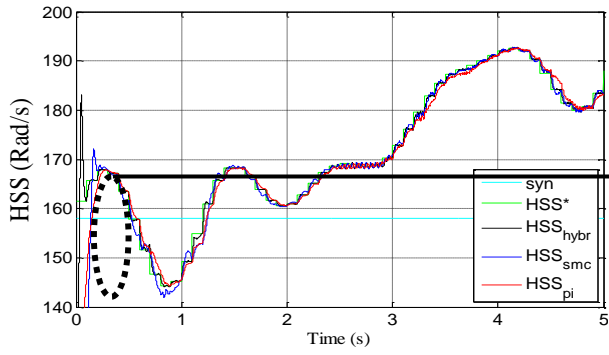
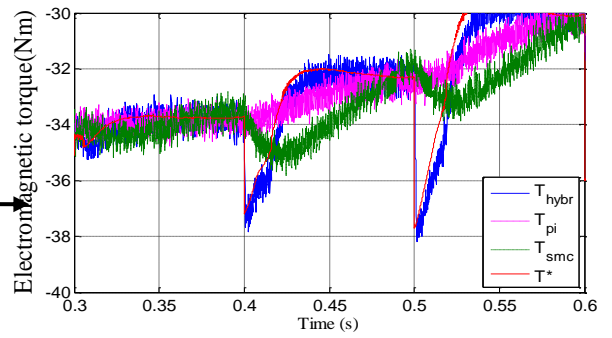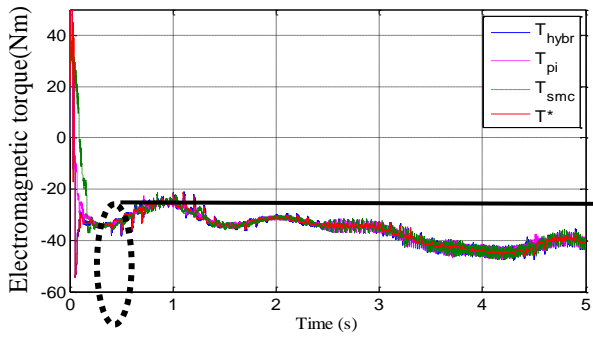Fig 2.   High Speed Shaft Tracking

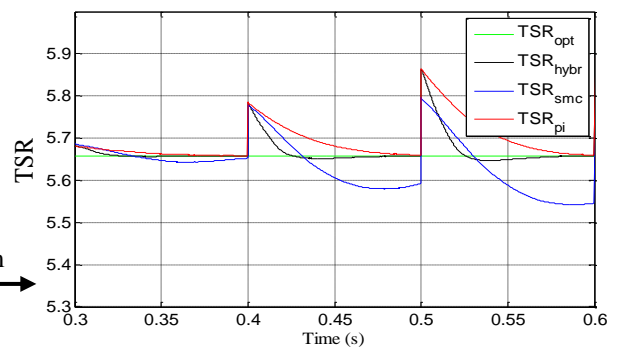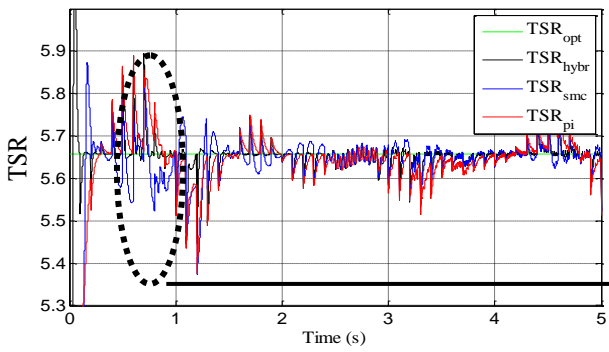**Fig. 1**

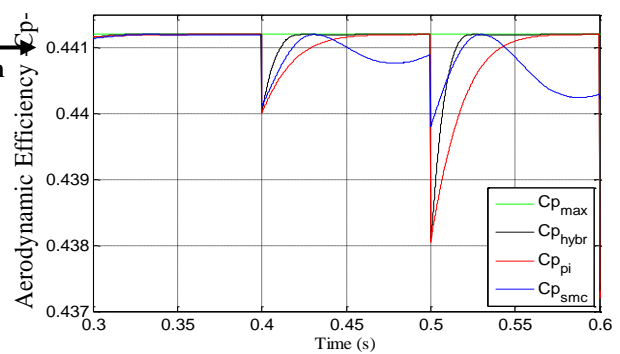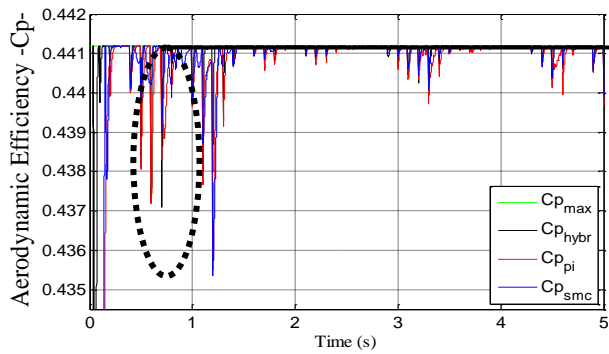Fig 3.   Electromagnetic Torque Tracking

Fig 4.   Tip Speed Ratio (λ)

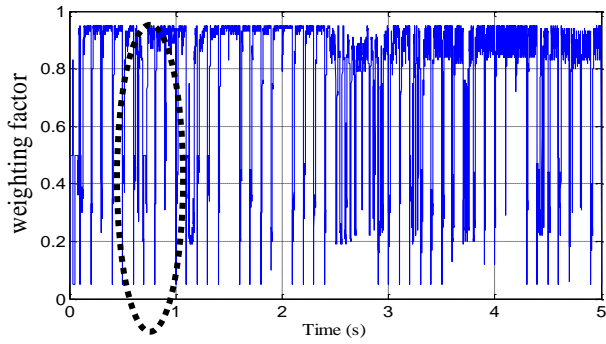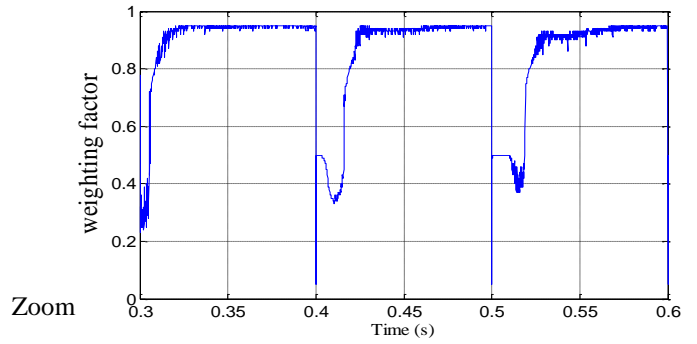Fig 5.   Aerodynamic Efficiency (Cp)

Zoom
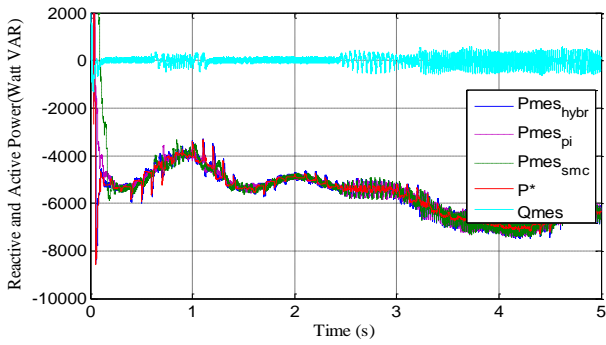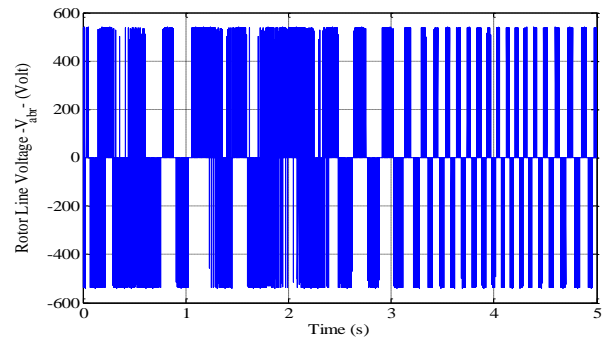
Fig 6.   Supervisor decision (δ)

Fig 7.   Stator active and reactive powers.

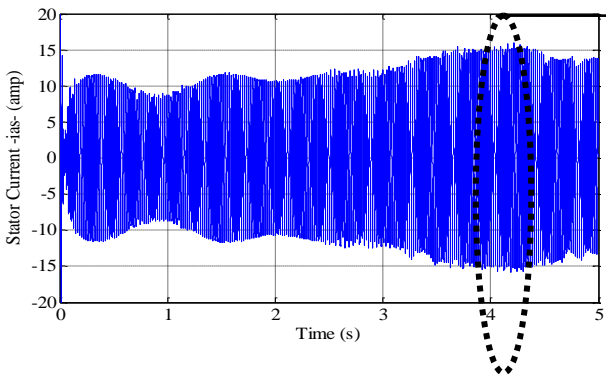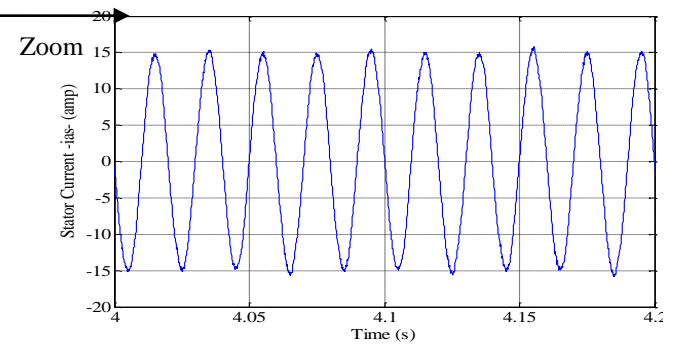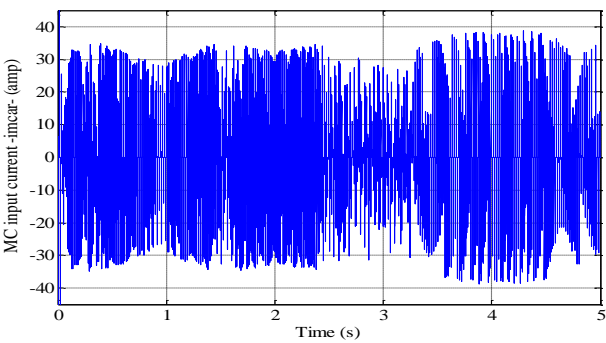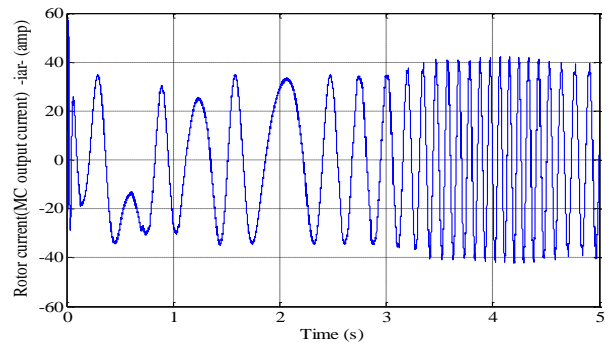Fig 10.   Rotor line Voltage vabr

Zoom

Fig 8.   Stator Current ias

(a) iari

(b) iar

Fig 9.   (a) MC input (filter side) and (b) output
(rotor side) currents

(a) sub-synchronous regime
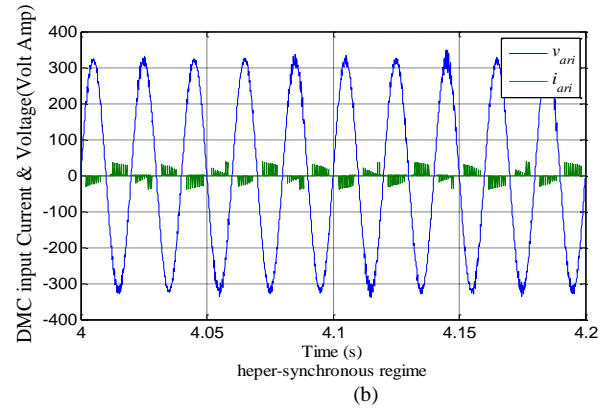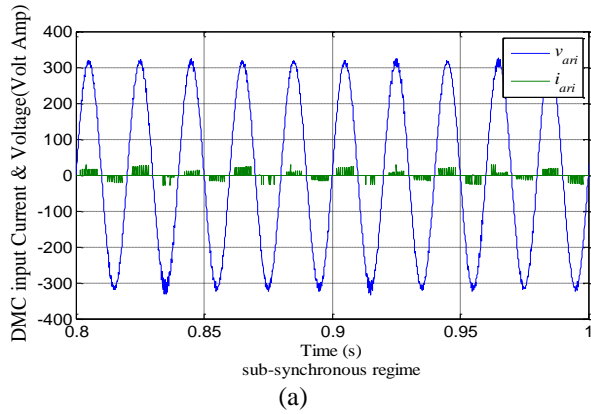
(b) heper-synchronous regime
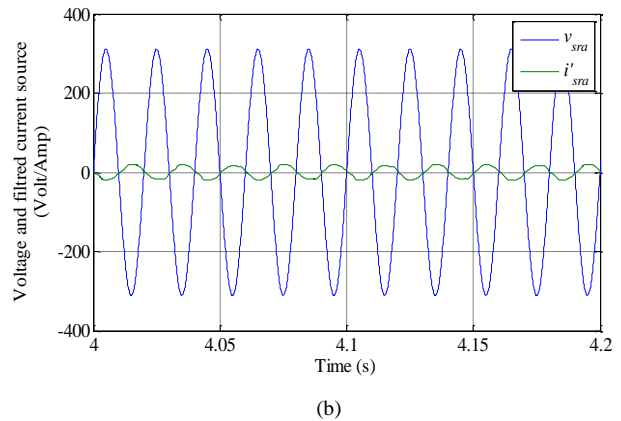
Fig 11.   MC input voltage versus current.

(a)

(b)
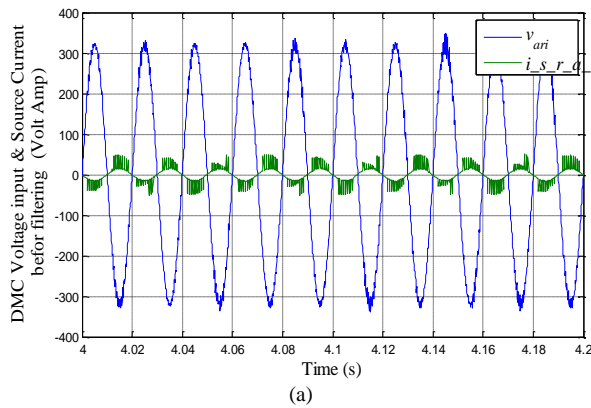
Fig 12.   Current isra (a before filtering) and Current isra'(b after filtering)

$THD(i_{asr})=0.4808$

$THD(i'_{asr})=0.0482$

(a)

(b)

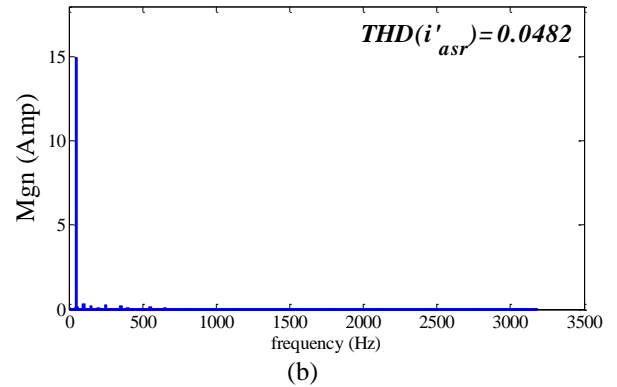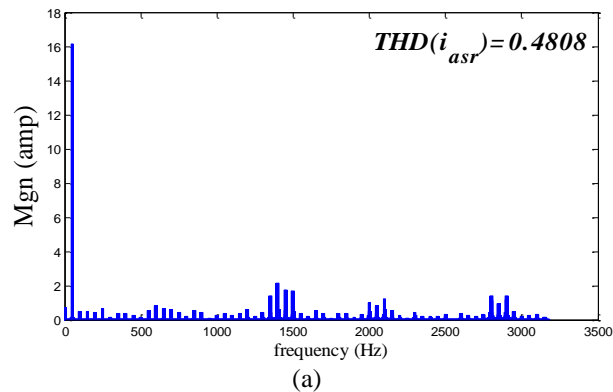Fig 13.   Figure 29.(a) THD of unfiltered current isra, (b)THD of filtered current isra'

5 Conclusion

In this paper, a hybrid controller for wind speed of WECS is designed to track efficiently the maximum power point. The designed controller combines the merits of sliding mode control to those of PI control to obtain an optimal regime generation. The method uses a fuzzy logic supervisor to switch between the two modes.

The studied WECS based DFIG replaces the classic back to back converters topology by a matrix converter well suited for this application. The indirect space vector modulation SVM is applied to MC. Then, a RLC filter is designed to enhance power quality in the grid side by reducing the THD of grid current and voltage.

Over the different simulation results, it is observed that the performance of the WECS system are enhanced in

term of fast tracking speed, low torque ripples, high efficiency, less oscillations around optimal power points and low current and voltage distortion in the grid side.

Appendix

The system used for validations has the following features:

Type: fixed pitch HAWT turbine based (high speed): rated wind speed Vr = 9.5 m/s, R=3 m.

Energetic performance: maximal value of the power coefficient Cpmax =0.44 at optimal tip speed ratio λopt= 5.65.

Constant air density: ρ=1.25 Kg/m3

Electromechanical features: Jt=0.1 Kg.m2, D= 6,73.10-3 N.m.s-1

Gearbox coefficient G=10.

Generator parameters:

Rs=0,455 Ω ; Rr=0,62 Ω ; Ls=0,084 H ; Lr=0,081 H ; M= 0.078 H ; 50 Hz,

380 V, Pn=7.5 kW, Nn=1440 rpm.

References

[1] I. Munteanu et al. "optimal control of wind energy systems, towards a global approach", Springer-Verlag edition, p.22-31-41-47-48-75-129, London2008.
I. Munteanu, S. Bacha, A. I. Bratcu, and D. Roye, "Energy-Reliability Optimization of Wind Energy Conversion Systems by Sliding Mode Control", IEEE Trans. On energy conversion, p.975-977-978-979, vol. 23, N°.3, sept. 2008.

[2] Z. Chen, J. Guerrero, and F. Blaabjerg, "A review of the state of the art of power electronics for wind turbines," IEEE Trans. Power Electron., vol. 24, no. 8, pp. 1859 –1865, Aug. 2009.

[3] F. Akel, T. Ghennam, E.M. Berkouk, M. Laour, "An improved sensorless decoupled power control scheme of grid connected variable speed wind turbine generator". Energy Conversion and Managementjournal, vol. 78, p. 584-586, 2014.

[4] T. Ackermann, "Wind Power in Power Systems," John Wiley & Sons Ltd, p-527-562-570Stockholm, Sweden, 2005.

[5] G. Abad, J. L. Miguel, A. R. L. Marroyo, ''Doubly fed induction machine,'' John Wiley & Sons, Inc, New Jersey,2011.

[6] M. P. Kazmierkowski; R. Krishnan; F. Blaabjerg; "Control in power electronics", Academic Press Series In Engineering, Elsevier Science (USA),2002.

[7] P. W. Wheeler, H. Zhang, D. A. Grant, "A theoretical and practical consideration of optimized input filter design for a low loss matrix converter," in proc. on Fifth International Conference on Power Electronics and Variable-Speed Drives, vol., no., pp. 363-367, Oct 1994.

[8] H. She, H. Lin, X. Wang and L. Yue, "Damped input filter design of matrix converter," International Conference on Power Electronics and Drive Systems, 2009. PEDS 2009., pp.672-677, 2-5 Nov. 2009.

[9] T. F. Podlesak and D. Katsis, "A 150 kVA vector controlled matrix converter induction motor drive," Industry Applications Conference, 39th IAS annual meeting. conference record of the 2004 IEEE, vol. 3, pp. 1811- 1816, Oct. 2004.

[10] M. Odavic, M. Sumner, P. Zanchetta and J. C. Clare, "A theoretical analysis of the harmonic content of PWM waveforms for multiple-frequency modulators," IEEE Transactions on Power Electronics, vol. 25, no. 1, pp. 131-141, Jan. 2010.